PHYSICAL REVIEW B VOLUME 1, NUMBER 12 15 JUNE 1970

Photoconductivity and Density of States for Amorphous GeTe†

W. E. Howard and R. Tsu

IBM Thomas J. Watson Research Center, Yorktown Heights, New York 10598

(Received 8 January 1970)

GeTe films evaporated onto substrates held at room temperature are amorphous and exhibit properties more characteristic of chalcogenide glasses than of crystalline GeTe. The resistivity of such films increases exponentially with reciprocal temperature, the activation energy being 0.30–0.35 eV. We have measured both optical absorption and photoconductivity for these films over a wide range of temperatures. The absorption coefficient is found to vary as $(h\nu - E)^2/h\nu$ at higher photon energies, E_g being 0.70 eV at 295 °K and 0.77 eV at 77 °K, while at lower photon energies the absorption follows an exponential variation with slope independent of temperature. These results are used to infer a density of states for amorphous GeTe. Photoconductivity is observed down to photon energies of 0.2 eV near room temperature; however, the strong temperature dependence of photoconductivity for photon energies below about 0.6 eV distinguishes the response in this region as arising from a different mechanism from that for photon energies greater than E_g. The observed magnitudes of photoresponse, rise times, and intensity dependences are seen to be consistent with a Mott-Cohen model using the inferred density of states. It is proposed that the observed low-energy photoconductivity may result from a perturbation of the mobility edge by trapped charge.

INTRODUCTION

GeTe films evaporated onto substrates held at temperatures below about 100 °C have properties strikingly different from those of films evaporated with higher substrate temperatures.[1,2] The latter films, which we have studied extensively,[3] are polycrystalline, and like GeTe crystals pulled from the melt, they are strongly degenerate p-type semiconductors with nearly metallic behavior, including resistivities $\sim 10^{-4}$ Ω cm at room temperature. In contrast to this, the former films exhibit intrinsic semiconductor behavior with resistivities which vary exponentially with inverse temperature and which are the order of 10^3 Ω cm at room temperature. In addition, simple powder camera x-ray measurements show no evidence of crystallinity in these films.

It is known from the studies of Hilton *et al.*[4] that GeTe does not form a glass when quenched from the melt, as do many chalcogenide mixtures and compounds. On the other hand, the similarity of properties of these GeTe films to those of the general class of chalcogenide glasses[5-8] leads us to assume that we are dealing with vapor-quenched "amorphous" films. There are, in fact, some data on the structure of such films. Bahl and Chopra[9] have determined a radial distribution function from electron diffraction measurements and find it to be the same as in crystalline GeTe. However, Bienenstock and Betts[10] have concluded from x-ray diffraction measurements of Ge-Te alloys other than GeTe that the structure has short-range order different from that of crystalline material. One might hope that soon this question would be resolved. {*Note added in proof* . A recent publication [D. B. Dove, M. B. Heritage, K. L. Chopra, and S. K. Bahl, J. Appl. Phys. Letters 16, 138 (1970)] reports that the short-range structure of amorphous GeTe is not the same as that of crystalline GeTe}. The experiments are complicated by the fact that an electron beam can possibly produce some crystallization. Having acknowledged the structural uncertainties, we use the word "amorphous" to distinguish our films from crystalline GeTe films with appropriate reservations being implied.

Our emphasis at this point must then be on amorphous GeTe as a disordered semiconductor without any *a priori* relationship to crystalline GeTe other than the similarity of their compositions. We shall describe herein some of the properties of amorphous GeTe, with an emphasis on optical properties, and draw some inferences from these about the electronic density of states. Our feeling is that one needs some sort of reasonable estimate of the density of states as a starting point for the interpretation of more complex properties such as electrical transport.

It may be noted that GeTe is very well suited for general studies in that it is easily evaporated thermally in the form of a molecular vapor. It is, consequently, not susceptible to compositional uncertainties, and provides reproducible results with relatively little effort. Since GeTe possesses these experimental advantages and since it also exhibits properties characteristic of the class of disordered chalcogenides which have recently at-

tracted considerable practical interest,[11] we feel that a thorough understanding of the properties of amorphous GeTe would be a useful step toward an understanding of the larger class of materials.

SAMPLE PREPARATION

Films were prepared by thermal evaporation of Ge-rich GeTe using resistance or electron beam heating. The Ge-rich source was used to minimize the vapor pressure of Te_2, as suggested by the results of Brebrick.[12] Both NaCl and sapphire substrates were used and films were deposited in thicknesses of 0.3 μ to 16 μ. We have mentioned that the evaporation of GeTe is a straightforward process. This is because the vapor pressure is relatively high at, say, 600 °C and the vapor is predominantly the species GeTe. On the basis of equilibrium studies of GeTe[12] one would expect some excess of Te in evaporated films, the upper limit being about 53-at.% Te and the excess being rather insensitive to source temperature. On the other hand, precise chemical analyses of evaporated GeTe by Ch'un-hua *et al.*[13] yielded stoichiometric compositions to within ~ 0.1%. An analysis of one of our films yielded (50.7 ± 2.5)-at.% Te.

Most films were deposited onto substrates held at room temperature, although some were prepared at elevated temperatures. For substrate temperatures greater than about 50 °C, film properties such as refractive index begin to differ, suggesting that partial crystallization may take place under those conditions. Evaporated electrodes of gold or molybdenum were used for conductivity measurements. On the basis of four terminal measurements and variations of sample resistance with film thickness and electrode geometry, we concluded that the sample resistances were dominated by film resistivity as opposed to contact resistances. The films are Ohmic for the range of electric fields used in the present experiments. Gold electrodes are not desirable for measurements at elevated temperatures because the gold apparently diffuses rather rapidly into amorphous GeTe. This is seen by the fact that regions near the contacts are stabilized and do not crystallize at the same temperature as the rest of the films.

EXPERIMENTS

Electrical Measurements

Figure 1 shows the temperature dependence of the resistivity for amorphous GeTe. Note first that the resistivity at room temperature is about 10^3 Ω cm. This is nearly seven orders of magnitude greater than the resistivity of crystalline GeTe at room temperature. The resistance variation is approximately exponential, with an activation energy of 0.3–0.35 eV. That is, if one looks closely at such a curve, it is possible to distinguish several regions of slightly different activation energies, as indicated on the figure. These slight variations have yet an unclear origin, but they may be useful at some later time to distinguish regions having different mechanisms of conduction. That is, at low temperatures conduction may proceed by dc hopping with electric-field-dependent transition probabilities , while at high temperatures it may be more appropriate to describe conduction as a two stage process of thermal excitation with band mobility. In both cases, the activation energy could be approximately the same.

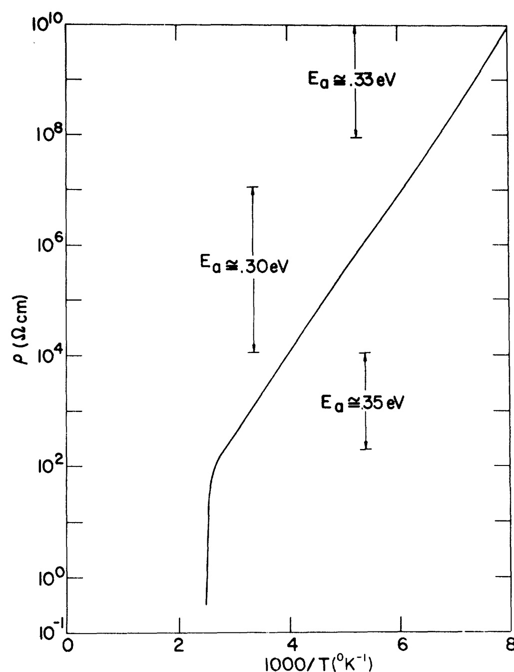

FIG. 1. Resistivity versus reciprocal temperature for typical amorphous GeTe film. Horizontal markers connected by arrows are intended to distinguish portions of the curve having slightly differing slopes, the slopes being indicated by their equivalent activation energies in electron volts. The sharp drop in resistivity to the left represents the onset of crystallization.

Figure 1 represents a variation of resistivity measured over a period of approximately an hour. The region where annealing begins to take place is measured within a period of a few minutes. However, above room temperature there is a tendency for the films to anneal to higher resistivity in the way that has been studied in detail in other amorphous semiconductors such as Ge and Si.[14-16] Below room temperature the films are stable. As the temperature increases to (120 ± 10) °C, the films

crystallize, and in time the sample resistance decreases by several orders of magnitude. (Generally, some cracking of the film occurs during crystallization, so that one does not reach the conductance expected for crystalline GeTe.) The crystallization is not rapid, and therefore not well defined in temperature for runs taking only of the order of 1 h over all. One can easily stop the crystallization process by recooling. If one examines a partially crystallized film optically, the crystalline regions are clearly distinguished by a difference in reflectivity in the visible crystalline GeTe having nearly metallic reflectivity. One can see then that crystallization occurs by nucleation and growth of roughly circular crystalline regions starting from a density of centers of the order of $10^4/cm^2$. For films thicker than a few thousand angstroms there are noticeable tension cracks which develop upon crystallization, and usually the cracking is accompanied by peeling of the crystalline regions. On the basis of the size of the cracks one can estimate that crystalline GeTe is more dense than amorphous GeTe by 5–10%.

We are unable to detect a Hall voltage using a dc magnetic field of 10^4 Oe.

Optical Absorption

We measured reflectance and transmission for some of our films on NaCl substrates. The absorption coefficient α was obtained from these data, taking into account the effect of the substrate (see, for example, Ref. 3). Figure 2 shows a semilog plot of α versus $h\nu$ for two temperatures. It is apparent from this plot that the absorption coefficient has an exponential tail, at least down to about 0.5 eV. The slope of the exponential is the same at both temperatures and is equal to 11.5 ± 1.0 eV^{-1}. At higher photon energies, $\alpha \propto (h\nu - E_g)^2/h\nu$ as can be seen from a plot of $(\alpha h\nu)^{1/2}$ versus $h\nu$ (see Fig. 3), the intercept of which defines an energy gap E_g. We obtain values for E_g of 0.70 eV at 295 °K and 0.77 eV at 77 °K. The absorption coefficient for crystalline GeTe in the same range of photon energies is nearly an order of magnitude greater.[3] The optical dielectric constant determined from interference fringes is approximately 11 for amorphous GeTe. This also is quite different from the value of 37 for crystalline GeTe[3] and suggests that one should not expect a simple correlation between crystalline and amorphous GeTe.

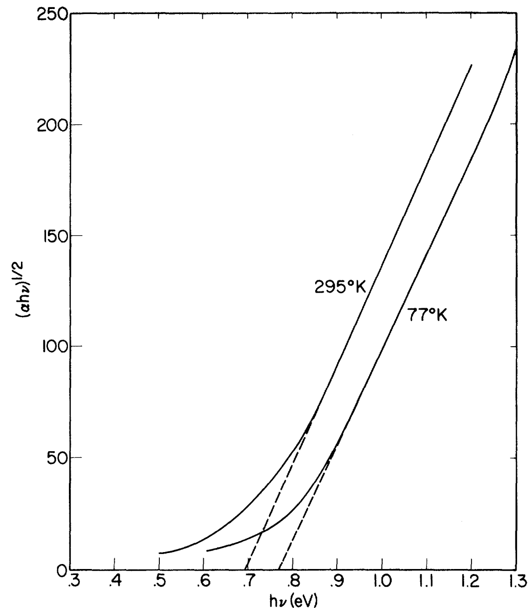

FIG. 3. Square root of the product of absorption coefficient and photon energy, versus photon energy, for two temperatures. Dashed lines are extrapolations of straight-line portions of the curves at higher photon energies. The intercepts so obtained are 0.70 and 0.77 eV for 295 and 77 °K, respectively.

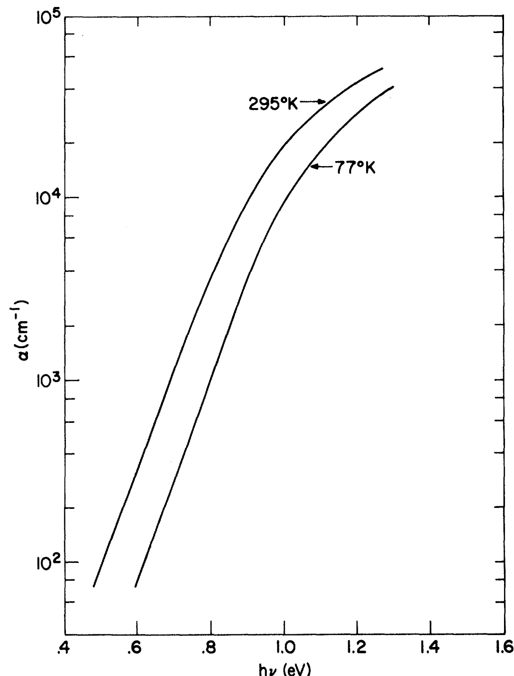

FIG. 2. Absorption coefficient versus photon energy for amorphous GeTe films measured at two temperatures.

Photoconductivity

Figure 4 is a plot of the log of photocurrent per incident photon versus photon energy, at several temperatures, for a typical sample. Here the photocurrent is measured using a lock-in amplifier

and a chopping frequency of $6\frac{2}{3}$ cps. Near room temperature, one can see that, as with the optical absorption, there is also an exponential tail to the spectral dependence of photoconductivity, with measurable photoconductivity down to photon energies of less than 0.2 eV. It should be noted that this is less than the activation energy for conductivity, which suggests that photoconductivity at lower photon energy is due to a different mechanism, involving localized states. The slope of the exponential tail is significantly smaller than the slope of $\ln\alpha$ versus $h\nu$, the former being about 7.5 eV^{-1} at room temperature and the latter being 11.5 eV^{-1}.

As the figure shows, the low-energy photoconductivity disappears rapidly upon cooling. For temperatures near room temperature and for photon energies greater than 0.8 eV, the photoconductivity is relatively independent of photon energy. In fact, what energy dependence persists can be attributed to the presence of some bolometer action, or sample heating, at these temperatures (see below).

At lower temperatures, the shape of the photoconductivity curve in the vicinity of the edge approaches that of the absorptance versus photon energy as obtained from transmission and reflectance measurements. However, for these temperatures, the spectral response is not reproducible in detail from sample to sample. For example, the small rise in photoconductivity at 127 °K for photon energies greater than 1.2 eV (shown in Fig. 4) is not seen in all samples.

One can see from the figure that photoconductivity is not a monotonic function of temperature above the absorption edge. Figure 5 shows the same information as a plot of photoconductivity versus temperature for two photon energies. For $h\nu = 1.15$ eV, the photoconductivity rises as a roughly exponential function of temperature to a peak at approximately 180 °K, after which it dips to a local minimum at 230 °K and rises again to room temperature. At 0.3 eV, as mentioned, the photoconductivity simply decreases rapidly with decreasing temperature from room temperature.

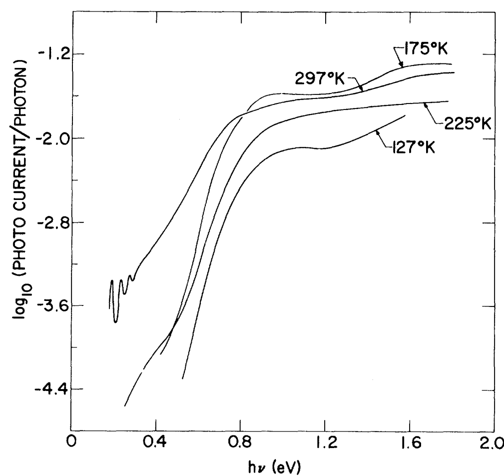

FIG. 4. Photocurrent per incident photon versus photon energy for a typical amorphous GeTe film measured at several temperatures. The structure seen at low photon energies and 297 °K is due to interference fringes in the film.

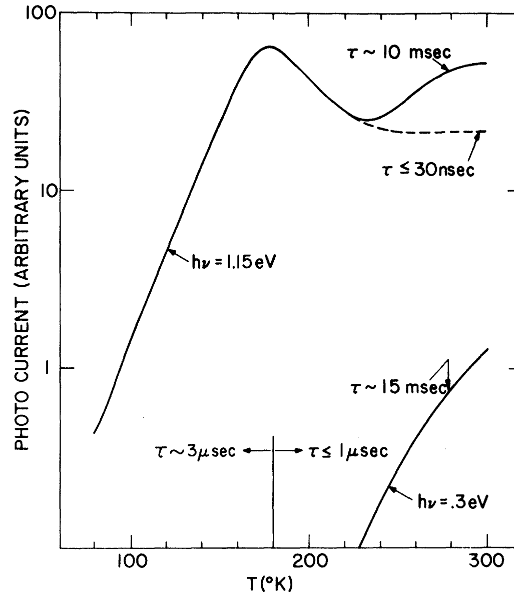

FIG. 5. Photocurrent versus temperature for two photon energies 1.15 and 0.3 eV. Solid curves represent essentially the steady-state photocurrent. The dashed portion of the upper curve represents a fast component of photoconductivity having a rise time of less than 30 nsec at room temperature. The total photoconductivity near room temperature for the same photon energy includes a slow component with rise time of approximately 10 msec. The rise time of the fast component changes with temperature, as indicated at the bottom of the figure (see text).

Using a GaAs laser, we have examined the transient behavior of the photoconductivity at 1.47 eV. Figure 6(a) shows a typical waveform at room temperature. There is a fast rise followed by a slow component of photoconductivity having a rise time of the order of 10 msec. The rise time of the fast component was found in all cases near room temperature to be limited by the *RC* time constant associated with the sample capacitance and the current sampling resistor. By using sampling techniques and pulse averaging, we were able to reduce this rise time to 30 nsec. Since the laser rise time was less than 10 nsec, we can say that the photoconductive lifetime of the fast component

is less than or equal to 30 nsec. In Fig. 5 the dashed curve represents the variation of the fast rise time component in the vicinity of room temperature.

We have concluded that for $h\nu > 1$ eV, the slow component of photoconductivity near room temperature is due predominantly to sample heating on the basis of several considerations: (a) Order-of-magnitude calculations of the temperature rise and the thermal time constant expected for our films give values consistent with the experimental results. (b) By changing the geometry of the light beam, we are able to change the slow rise time of photoconductivity in a way that is consistent with a change in thermal time constant. (c) The disappearance of the slow component with cooling is consistent with the expected decrease of $d\sigma/dT$ with temperature, this being the basis of the effect.

This understanding of the role of heating allows us to conclude, on the other hand, that the long-wavelength photoconductivity *cannot* be due only to heating, as the absorptance of the samples is not sufficiently great as those wavelengths. The long-wavelength response is then largely a true photoconductivity. This can also be seen from rise time measurements (see below).

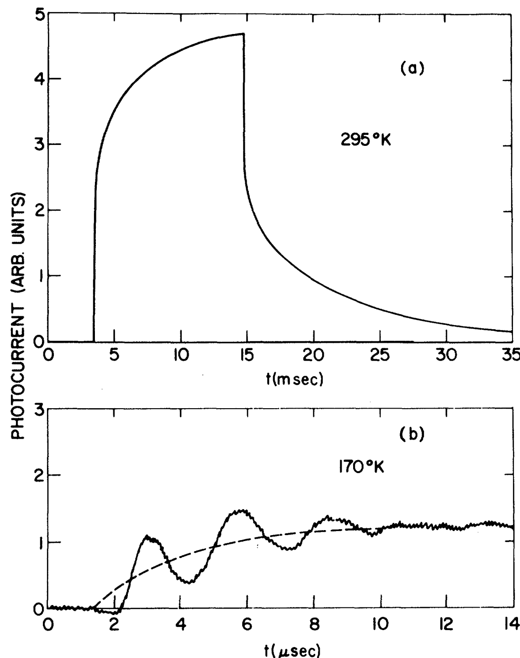

FIG. 6. Photocurrent waveforms at two temperatures illustrating the following: (a) the response at 295 °K consisting of a fast step followed by a slow rise with rise time of the order of 10 msec, and (b) the simple fast response at 170 °K with rise time of approximately 3 μsec (the ringing is due to pickup from the laser circuit).

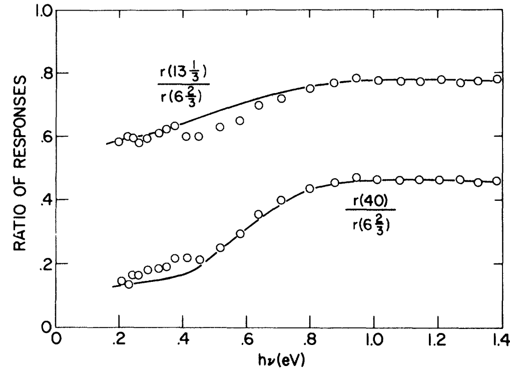

FIG. 7. Ratios of photoconductive responses for two pairs of chopper frequencies, versus photon energy, used to determine rise times for weak photoconductivity signals.

Returning to Fig. 5, the fast rise times indicated were actually measured at 1.47 eV with the GaAs laser, although in the interest of a more accurate temperature dependence, the photocurrent was measured at 1.15 eV using an incandescent tungsten source. Results such as those of Fig. 4 indicate that this should not make any significant difference in conclusions. The indications of regions of rise time are to be understood in the following way: As the sample is cooled, the slow component (~ 10 msec) essentially disappears, although there always remains a component with $\tau \sim 1$ msec which amounts to a few percent of the response. From room temperature to about (180 ± 20) °K, the rise time of the major component of photoconductivity is measurement limited to about 1 μsec, however, starting at about 220 °K one can see a component with somewhat slower rise time. In the region of 180 °K, the photoconductivity very quickly becomes dominated by a component with rise time of approximately 3 μsec, and this appears to remain constant down to about 140 °K which is as far as we can measure rise times. Figure 6(b) gives an indication of how imprecise these measurements are, the ringing being due to pickup from the laser, even with considerable shielding.

At 0.3 eV the signal is too weak (using a Globar source) to measure the rise time directly, so the rise time of ~ 10 msec is based upon measurements at several chopping frequencies. The photoconductivity waveforms at, say, $h\nu = 1$ eV can be fitted very well by curves consisting of a step plus a simple rise time curve going as $(1-e^{-t/\tau})$. Assuming that the response at lower photon energies follows the same form, then the dependence of photocurrent on chopping frequency is predictable.

Specifically, if the response R is given by

$$R(t)=A+B(1-e^{-t/\tau}), \qquad 0<t\le\tfrac{1}{2}T$$
$$=B(e^{-(t-T/2)/\tau}-e^{-T/2\tau}), \qquad \tfrac{1}{2}T<t\le T \qquad (1)$$

where τ is the slow rise time and T is the chopper period, then the sine transform $r(\omega)$ as measured by a lock-in amplifier will be given by

$$r(\omega)=A/\pi+(B/\pi)\left[(1+e^{-\pi/\omega\tau})/(1+\omega^2\tau^2)\right], \qquad (2)$$

where ω is the chopping frequency. At least three chopping frequencies must be used to determine A, B, and τ.

By making measurements at $6\frac{2}{3}$, $13\frac{1}{3}$, and 40 cps we obtain results which are typified by Fig. 7. These can be seen to demonstrate the following properties: (i) At higher photon energies, in the region of total absorption, both the time constant τ and the ratio of fast to slow components are independent of photon energy; however, both quantities depend upon the size of the incident light spot, as we mentioned in the discussion of bolometer effect. Furthermore, the results in this region of photon energies using the chopper-frequency technique are in agreement with direct waveform measurements. (ii) The fast component apparently disappears at about 0.45 eV, i.e., in the expressions above $A/B<0.05$ below 0.45 eV. (iii) For light-spot sizes yielding a relatively short thermal time constant, say 6 msec, the time constant increases steadily with decreasing photon energy below 0.9 eV to a value of about 14 msec at 0.2 eV. (iv) For larger light spots leading to thermal time constants of 10–12 msec, the time constant stays fixed to lower photon energies, but by 0.2 eV it has increased to the same value of 14 msec. This constitutes additional evidence that

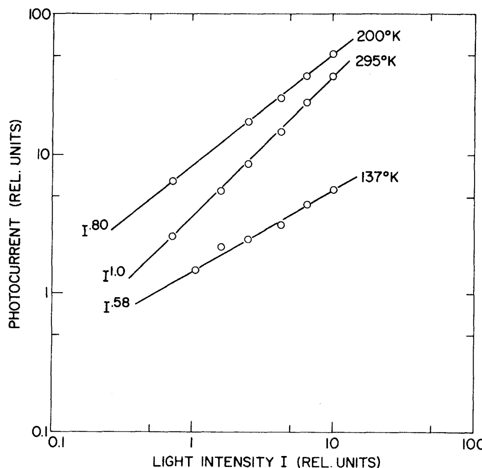

FIG. 8. Dependence of photocurrent on light intensity for $h\nu=1.47$ eV measured at several temperatures. The straight lines correspond to power laws, as indicated.

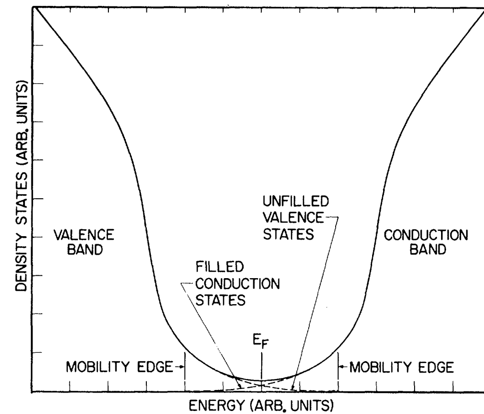

FIG. 9. Schematic representation of the Mott model for amorphous semiconductors, in terms of a one-electron density-of-states variation with energy. The mobility edges are the boundaries between nonlocalized band states and localized states in the pseudogap. Dashed curves indicate a separation of the midgap states into distinct overlapping conduction band and valence band states, as suggested by Cohen *et al.* (Ref. 17).

the photoconductive response at low photon energies is not a bolometer effect.

At room temperature, photoconductivity is linearly dependent upon light intensity, as determined at several photon energies covering the range of response (0.4, 1.15, and 1.47 eV). As the temperature is lowered, the response becomes sublinear, as shown in Fig. 8 for $h\nu=1.47$ eV. As indicated, the response approaches a square-root dependence below 140 °K, although at lower temperature the results are increasingly less accurate due to low signal levels. The intensity dependence is roughly independent of photon energy, although at lower temperatures the response is closer to a square-root law for lower photon energies.

Although Figs. 4 and 5 show relative photoconductivity, we have also determined approximately the absolute response at one wavelength. If the change in sheet conductivity with illumination is taken as

$$\sigma_s=AFq\mu\tau, \qquad (3)$$

where A is the absorptance and F is the light flux in photons/cm^2 sec, then the product $\mu\tau$ is equal to 1.2×10^{-10} cm^2/V for the fast component at 1.47 eV and room temperature.

DISCUSSION

We take as a starting point for our discussion the model for amorphous semiconductors attributed to Mott,[17] in which there is assumed to be not only a tailing of valence and conduction band states into a pseudogap as a result of the disorder,

but also an abrupt change in the character of these states at particular energies, thus giving rise to a "mobility edge" and a well-defined energy gap for conduction. Figure 9 shows a schematic view of this model in terms of a one-electron density of states. We have added as dashed lines the modification proposed by Cohen *et al.*[18] in which is emphasized the distinguishability of valence and conduction states in the midgap region. While some of our analysis implicitly uses this distinguishability, the necessity of it is not at all clear in terms of comparison with experiment.

The major fact which the Mott model accommodates is the rather constant activation energy over a wide range of temperature. The further result in our case that the activation energy of 0.3–0.35 eV is of the order of one-half the energy gap from optical absorption, leads one to think in terms of a more or less symmetrical distribution of states for which the minimum density of states is still sufficiently great to stabilize the Fermi energy. Of course, we do not know *a priori* the relationship between the optical absorption energy gap and the mobility gap, so that the Fermi energy could be shifted toward one mobility edge. In fact, field-effect measurements on amorphous GeTe by Stiles and Howard indicate p-type conduction.[19] Nevertheless, we have found it useful in considering the interband optical absorption to assume a symmet-

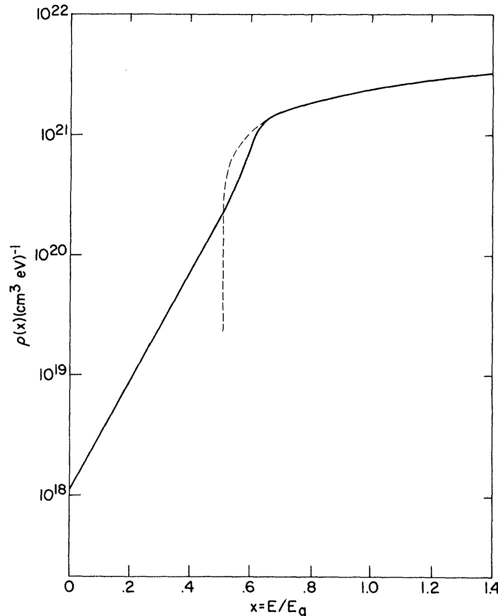

FIG. 10. Density of states for amorphous GeTe versus reduced energy, measured from midgap, as inferred from optical absorption. Dashed curve represents the extrapolated density of states for parabolic band.

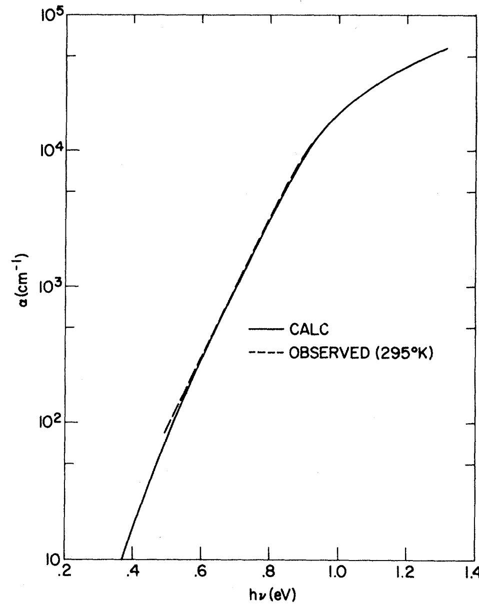

FIG. 11. Absorption coefficient expected on the basis of the density of states of Fig. 10 versus photon energy. The observed absorption coefficient is shown as a dashed curve primarily to indicate that the lower limit of the measurements was approximately 0.5 eV. Above 0.9 eV the dashed curve falls on the solid curve.

rical density-of-states distribution, while keeping in mind the possible consequences of asymmetry.

Because the energy dependence of the observed optical absorption approaches that expected for parabolic bands at higher photon energies, and exhibits an exponential tailing at lower photon energies which is independent of temperature (i.e., not an Urbach-type absorption tail[20]), we are led to calculate what absorption one would expect between bands with density-of-states tails. In a material with no long-range order, it is generally considered that crystal momentum k is no longer a good quantum number; therefore, conservation of crystal momentum is no longer required and all transitions are allowed, as with the case of allowed indirect transitions in a crystal. We choose to formulate this idea in the following way: Assume, by analogy with Bloch states, that we can write the valence band states as

$$\psi_{ik} = \sum_{R_j} u_v(r - R_j) f_{ik}(R_j), \qquad (4)$$

where $u_v(r - R_j)$ is essentially a molecular wave function centered on a molecular unit at R_j, and the functions $f_{ik}(R_j)$ are an orthonormal set of envelope functions, the k being used here merely as an index. That is,

$$\sum_{R_j} f^*_{ik}(R_j) f_{ik'}(R_j) = \delta_{kk'} . \qquad (5)$$

In the same way we write the conduction states as

$$\psi_{fk}=\sum_{R_j} u_c(r-R_j)f_{fk}(R_j). \qquad (6)$$

The assumption that all transitions are equally probable can then be introduced by assuming that a given envelope function of the valence band is composed of equal fractions of all conduction band envelope functions, i.e., for all k and k'

$$\sum_{j=1}^{N} f_{fk}^{*}(R_j)f_{ik'}(R_j)=\frac{1}{\sqrt{(2N)}} \qquad (7)$$

since there are $2N$ k values per band. The justification for this assumption of equal transition probabilities rests most strongly on the observation of photoconductivity down to low photon energies, since photoconductivity requires absorption and a rapidly vanishing matrix element would imply very low absorption at low photon energies leading to a rapidly increasing $\mu\tau$ product with decreasing photon energy. Further, the densities of states inferred on the basis of this assumption are consistent with there being appreciable overlap (see below).

If these assumptions are introduced into a standard calculation of optical absorption[21] between bands denoted by ψ_{ik} and $\psi_{fk'}$, then one obtains for the absorption coefficient α as a function of photon energy $h\nu$

$$\alpha=(2\pi^2e^2a^3\,\bar{p}^2/n\omega m^2c)\int_0^{h\nu} dE\,\rho_v(-E)\rho_c(h\nu-E), \qquad (8)$$

where $\bar{p}^2$ is the average of $(\vec{A}\cdot\vec{p})^2/A^2$, and $\rho_v(E)$ and $\rho_c(E)$ are the densities of states of the valence and conduction bands, respectively. If we assume now as mentioned above that the bands are symmetrical, i.e., that $\rho_v(-E)=\rho_c(E)\equiv\rho(E)$, then

$$\alpha(h\nu)=(2\pi^2e^2a^3\bar{p}^2/n\omega m^2c)\int_0^{h\nu} dE\,\rho(E)\rho(h\nu-E), \qquad (9)$$

or

$$\alpha h\nu\cong C\int_0^{h\nu} dE\,\rho(E)\rho(h\nu-E). \qquad (10)$$

Since α is known, this is an integral equation in ρ, which is solved directly by noting that if $\rho(E)\equiv 0$ for $E<0$, then this is simply the convolution integral for the Laplace transform and

$$\mathcal{L}(\rho(s))=[\mathcal{L}(\alpha h\nu)]^{1/2}. \qquad (11)$$

If $T(s)\equiv\mathcal{L}(\alpha h\nu)$, then

$$\rho(E)=(1/2\pi i)\int_{\sigma-i\infty}^{\sigma+i\infty} e^{sE}[T(s)]^{1/2}ds. \qquad (12)$$

The experimental results for $\alpha h\nu$ (Figs. 2 and 3) can be very well approximated by piecewise analytic functions which consist of high-energy portions going as $(h\nu-E_g)^2$ and tails going as $h\nu e^{\beta h\nu}$, the two portions of a given curve being matched smoothly at $h\nu/E_g=x_1$. In terms of $x\equiv h\nu/E_g$, this can be written

$$\begin{aligned}\alpha h\nu/E_g&=A(x-1)^2, && x\geq x_1\\ &=Ax[(x_1-1)^2/x_1]e^{a(x-x_1)}, && x\leq x_1\end{aligned} \qquad (13)$$

where $a=\beta E_g$. Then

$$\frac{T(s/E_g)}{AE_g}=e^{-sx_1}[s^2(x_1-1)^2+2(x_1-1)s+2]+\frac{(x_1-1)^2e^{-ax_1}}{x_1(a-s)^2}-\frac{(x_1-1)^2e^{-sx_1}}{x_1(a-s)^2}[1-(a-s)x_1]. \qquad (14)$$

This can be used to obtain $\rho(E)$ by numerical complex integration as indicated in Eq. (12) above. However, there are some difficulties in carrying this out. Strictly speaking, the real constant σ in the limits of integration of Eq. (12) should be chosen so that there are no branch points or singularities to the right of $s=\sigma$ in the complex plane. This guarantees that $\rho(E)=0$ for $E<0$, which is a consistency requirement. Unfortunately, the function T has an infinite set of branch points between $\mathrm{Re}(s)=8$ and $\mathrm{Re}(s)=9.5$. If one uses $\sigma>9.5$, the ρ obtained is nonphysical and oscillates wildly. This result can be seen to arise from the instability of the inverse Laplace transform.[22] Specifically, the behavior of T for large real s depends upon the behavior of α for small values of $h\nu$. We have no data for α at small photon energies, but essentially the numerical results tell us that the simple extrapolation of the exponential tail leads to a result which is mathematically correct but physically unacceptable. By choosing $\sigma=4$, for example, we relax the constraint on α at low energy and immediately obtain a stable density of states ρ. This ρ provides excellent agreement with the observed α in the range of our observations. The results for ρ (restored to physical units) are shown in Fig. 10 and the corresponding α is shown in Fig. 11, superimposed on the experimental results for α at room temperature. The absolute values of ρ given in Fig. 10 require a further assumption, namely, a magnitude for the quantity $\bar{p}^2$ in Eq. (16). We choose to use a value based on the results for crystalline GeTe [3] because amorphous GeTe is still GeTe and because from an order of magnitude point of view it is a typical value for interband momentum matrix elements in semiconductors. We take $\bar{p}^2/m=4.5$ eV, where m is the free-electron mass, this being about $\frac{2}{3}$ of the value for the transverse coupling in crystalline GeTe.

There are several points worth noting in Fig. 10. Above about 0.5 eV, the density of states approaches closely that for a parabolic band. Fur-

thermore, the magnitude of the density of states in this region corresponds to that for a band with effective mass equal to $0.7m$. This is both interesting and encouraging. It allows, for instance, the simple interpretation that at higher energies, the nonlocal carriers behave more or less like free particles. The total number of states below the parabolic edge is of the order of $2\times 10^{19}/\text{cm}^3$, which corresponds to a spatial separation of the order of 40 Å. Since for states with binding energies of the order of 0.1 eV one can estimate a minimum characteristic radius which is also of the order of 40 Å, there must, therefore, be some overlapping of states in the tail. A third point is the result that, in terms of distinct types of midgap states,[18] the number of unfilled valence states and the number of filled conduction states at 0 °K are both about $10^{17}/\text{cm}^3$.

In Fig. 11, one can see that while the theoretical results fit very well the exponential tail in the range of the experimental observations, the theoretical absorption decreases somewhat more rapidly at lower photon energies than an extrapolated simple exponential tail. This would be an interesting point to explore if there were available very thick samples of good quality.

It has already been mentioned that the photoconductivity versus photon energy (Fig. 4) is rather flat for higher photon energies, particularly when one discounts the contribution of sample heating. Also, the fractional magnitude of the fast component of photoconductivity at room temperature is constant above about 0.9 eV, as can be deduced from Fig. 4. The most straightforward interpretation here is that absorption at photon energies greater than 0.9 eV is followed by very rapid energy relaxation of photoexcited carriers to the mobility edge, i.e., to the lowest energy nonlocalized states, from whence they may recombine or become trapped.

While we are not yet in a position to establish a unique model of the dynamic processes in amorphous GeTe, it is interesting how much can be fitted into a rather simple picture based on the mobility edge concept and making use of our inferred density of states.

We start with the information that the temperature dependence of photoconductivity at 1.15 eV in Fig. 5 was measured with a light intensity which theoretically should produce a generation rate g averaged over the absorption length, of the order of $10^{23}/\text{cm}^3$ sec. Assume that carriers excited into nonlocalized states at the above rate (for simplicity we speak of electrons) very rapidly become trapped by the localized states near the mobility edge and assume that as far as these shallow traps are concerned there is a quasithermal equilibrium with the nonlocalized states. That is, assume that the population of trapped electrons n_t and the population of nonlocalized electrons n are related by having a common quasi-Fermi level. Assume further, in keeping with the model, that the recombination lifetime for nonlocal electrons is very much shorter than that for the localized, trapped electrons (this being the implication of the label "trapped").

Then, if the lifetime for nonlocalized carriers is τ, the steady-state relation is

$$n/\tau = g = 10^{23}/\text{cm}^3\,\text{sec} . \qquad (15)$$

Suppose that $\tau \sim 10^{-10}$ sec at room temperature, then $n \sim 10^{13}/\text{cm}^3$. However, for this density of nonlocalized electrons, we would expect a much greater density of trapped electrons. For instance, if we consider that the rapid trapping and thermalization takes place down to 0.2 eV below the mobility edge, we can calculate the ratio n_t/n using the density of states in Fig. 10, this ratio being relatively insensitive to the position of the mobility edge. For room temperature we find $n_t/n = 130$, i.e., $n_t = 1.3\times 10^{15}/\text{cm}^3$. This figure is consistent with the observation of the linearity of photoconductivity versus light at room temperature, because if we estimate the number of filled conduction states near the midgap, including the tail of the conduction band below midgap, we obtain a value $n_0 \sim 1.6\times 10^{17}/\text{cm}^3$. That is, these states are considered to be the main recombination centers at room temperature, since $n_0 \gg n_t$. It follows that in this region $\tau \propto 1/n_0$ and $i_{pc} \propto \mu g/n_0$. Since n_0 consists mostly of the tail overlap, it is relatively insensitive to temperature. The nonlocal or band mobility μ is, under these assumptions, of the order of 1 cm^2/V sec (from $\mu\tau = 1.2\times 10^{-10}\ \text{cm}^2/\text{V}$), but we know nothing of its temperature dependence except to expect that it should not be very strong, as in a hopping regime. The initial rise in photoconductivity with cooling represented by the dashed curve in Fig. 5 could then be attributed to an increase of mobility and/or a decrease of capture cross section. However, with cooling the major change expected would be in the number of the trapped carriers n_t, since the ratio

$$n_t/n \cong e^{+\Delta(1/kT-\beta)} , \qquad (16)$$

where Δ, the depth to which the traps are thermalized, is taken as 0.2 eV and β, the slope of the $\ln\rho$-versus-energy curve, is about 14.5 eV^{-1}.

By about 190 °K, n_t is comparable to n_0, and with further cooling n_t becomes much greater than n_0. Under this condition, the rise time for photoconductivity in the thermal trap case should be simply related to the lifetime by[23]

$$\tau_{\text{rise}} = (n_t + n)/n \;. \tag{17}$$

Consequently, τ_{rise} would be expected to increase from ~10 nsec at room temperature to ~3 μsec at 180 °K. We have pointed out in the previous section that the rise time does increase to about 3 μsec in this region of temperature. Also, as n_t becomes comparable to n_0, one would expect the trapped charges to become important recombination centers, so that photoconductivity would go from being linear with light intensity at room temperature to varying as the square root of light intensity below 150 °K. This, of course, is the observed tendency. In the low-temperature range, one would have

$$\tau \propto 1/n_t \,, \tag{18}$$

so that $$n_t \propto g\, e^{+\Delta[(1/kT)-\beta]}/n_t \;. \tag{19}$$

Then $$i_{pc} \propto \mu\, g^{1/2} e^{-\Delta[(1/kT)-\beta]/2} \tag{20}$$

and the photocurrent would be a strongly decreasing function with decreasing temperature. The observed variation does not fit well an exponential variation versus $1/T$, but above 120 °K it would fit best a curve with $\Delta = 0.17$ eV. This is to be compared with the initial assumption of $\Delta = 0.2$ eV.

One of the consequences of the above arguments which might be examined experimentally is the temperature dependence of luminescence from GeTe. If this is observable, there should be a predominance at room temperature of radiation with energy equal to half the energy gap, while with cooling there should be a change to a predominance of gap radiation below 180 °K. In the case of $As_2Te_3 - As_2Se_3$, luminescence has been reported[24] with two peaks at energies corresponding, approximately, to the energy gap and to one-half of the energy gap.

It may seem a contradiction to have assumed equal transition rates for all transitions in absorption while assuming that only nonlocalized carriers recombine rapidly. This can probably be reconciled by considering that N in Eq. (7) should not really be taken as the number of molecular cells in the sample but rather the number in some region characterized by a radius for overlapping localized states. Then everything can be renormalized without affecting the absorption. However, *recombination* of localized carriers would still require a spatial proximity and would thus be less likely than nonlocal to local recombination.

One aspect of the results which is not accommodated by the simple model used above is the long-wavelength photoconductivity near room temperature. Since, as mentioned in the previous section, the slope of the $\ln i_{pc}$-versus-$h\nu$ curve is smaller than the slope of $\ln\alpha$ versus $h\nu$ in the region where i_{pc} should be proportional to α, it follows that the photocurrent per photon increases with decreasing photon energy. In terms of one simple model in which all recombination takes place from nonlocalized states, the photocurrent per absorbed photon should be independent of energy. The rise time, on the other hand, is not inconsistent. We recall from the previous section that rise times for photoconductivity in the tail region were of the order of 10 msec. If the absorption of long-wavelength light is thought of as a direct generation of trapped carriers, then the rise time for photoconductivity can simply be the release time for thermal activation from traps to nonlocal states. The only possible explanation which we can think of for the behavior of the tail photoconductivity is to postulate that the large population of deep traps produced by the long-wavelength light produces a small perturbation of the mobility edge via a screening effect. The result of such a perturbation would be similar to the bolometer effect, an[illegible]ld also disappear rapidly with cooling. The trap population produced would be expected to increase with decreasing photon energy since more electrons are required in deeper states to produce the same nonlocal population n in the steady state. Thus the photocurrent per photon would increase with decreasing photon energy as observed.

In any event the long-wavelength photoconductivity merits more study, including the investigation of rise time versus temperature and possibly a direct observation of a change of activation energy with long-wavelength illumination. The difficulty in the former case is that the signal-to-noise ratio is already low for conventional infrared sources.

SUMMARY AND CONCLUSIONS

We have described some electrical and optical properties of amorphous GeTe films prepared by evaporation. Such films exhibit the exponential variation of resistivity with reciprocal temperature characteristic of intrinsic semiconductors. Both optical absorption and photoconductive response have exponential tails toward low photon energies. To this extent, the behavior of amorphous GeTe is typical of the general class of amorphous chalcogenides. However, in the case of the photoconductivity, the response at room temperature extends to photon energies of less than one-half the energy gap or, more significantly, less than the activation energy for conductivity. This low-energy photoconductivity, which has not been reported for other amorphous chalcogenides, disappears rapidly with cooling.

The slope of the exponential tail on the optical absorption is essentially independent of temperature, so we have used the absorption to infer a density of states for amorphous GeTe. Using this density of states, we have found that most of the photoconductivity results including temperature dependence, rise times, intensity dependence, etc., can be understood in terms of a Mott-Cohen model involving mobility edges and overlapping band tails. However, the behavior of the long-wavelength photoconductivity raises the possibility of another phenomenon, namely, the shifting of the mobility edges under the influence of large densities of trapped charge.

ACKNOWLEDGMENTS

We are pleased to acknowledge the contributions of a number of colleagues. Dr. D. F. O'Kane supplied us with source material for the films. We had the benefit of numerous discussions with Dr. M. H. Brodsky, Dr. L. Esaki, Dr. F. Stern, Dr. P. J. Stiles, and Dr. K. Weiser. We are grateful to M. H. Brodsky and K. Weiser for a critical reading of the manuscript. Finally, we wish to thank M. S. Christie and T. Hajos for valuable technical assistance.

---

†Work sponsored in part by the U.S. Army Research Office, Durham, N.C., under Contract No. DAHCO4-69-C-0069.

428 (1969); R. Tsu, W. E. Howard, and L. Esaki, in Proceedings of the International Conference on Amorphous and Liquid Semiconductors, Cambridge, 1969 (to be published).

[2]K. L. Chopra and S. K. Bahl, Bull. Am. Phys. Soc. 14, 98 (1969); J. Appl. Phys. 40, 4171 (1969); S. K. Bahl and K. L. Chopra, J. Vac. Sci. Technol. 6, 561 (1969).

[3]R. Tsu, W. E. Howard, and L. Esaki, Phys. Rev. 172, 779 (1968).

[4]A. R. Hilton, C. E. Jones, and M. Brau, Phys. Chem. Glasses 7, 105 (1966).

[5]T. N. Vengel and B. T. Kolomiets, Zh. Tekhn. Fiz. 27, 2484 (1957) [Soviet Phys. Tech. Phys. 2, 2314 (1957)].

[6]B. T. Kolomiets, Phys. Status Solidi 7, 359, (1964); 7, 713 (1964).

[7]J. T. Edmond, Brit. J. Appl. Phys. 17, 979 (1966).

[8]K. Weiser and M. H. Brodsky, Phys. Rev. B 1, 791 (1970).

[9]S. K. Bahl and K. L. Chopra, in Proceedings on Symposium Semiconductor Effects in Amorphous Solids, New York, 1969 (unpublished).

[10]A. Bienenstock and F. Betts, see Ref. 9.

[11]S. R. Ovshinsky, Phys. Rev. Letters 21, 1450 (1968).

[12]R. F. Brebrick, J. Chem. Phys. 41, 140 (1964).

[13]L. Ch'un-hua, A. S. Pashinkin, and A. V. Novoselova, Russ. J. Inorg. Chem. 7, 496 (1962).

[14]R. Grigorovici, N. Croitoru, A. Devenyi, and E. Teleman, in *Proceedings of the International Conference on the Physics of Semiconductors, Paris*, 1964 (Dunod, Paris, 1964), p. 423.

[15]P. A. Walley and A. K. Jonscher, Thin Solid Films 1, 367 (1968).

[16]R. Grigorovici, Mater. Res. Bull. 3, 13 (1968).

[17]See, for example, N. F. Mott, Festkoerperprobleme 9, 22 (1969).

[18]M. H. Cohen, H. Fritzsche, and S. R. Ovshinsky, Phys. Rev. Letters 22, 1065 (1969).

[19]P. J. Stiles and W. E. Howard (unpublished).

[20]F. Urbach, Phys. Rev. 92, 324 (1953).

[21]See, for example, L. I. Schiff, *Quantum Mechanics* (McGraw-Hill, New York, 1955), Chap. 10.

[22]R. Bellman, R. E. Kalaba, and J. A. Lockett, *Numerical Inversion of the Laplace Transform* (Elsevier, New York, 1966), p. 32.

[23]A. Rose, RCA Rev. 12, 362 (1951).

[24]B. T. Kolomiets, T. N. Manontova, and V. V. Negreskul, Phys. Status Solidi 27, K15 (1968).